Low-Order Modes as Diagnostics of Spheroidal Non-neutral Plasmas

M. D. Tinkle, R. G. Greaves, and C. M. Surko

Physics Department, University of California, San Diego, La Jolla, California 92093

R. L. Spencer and G. W. Mason

Department of Physics and Astronomy, Brigham Young University, Provo, Utah 84602

In many experiments on single-component plasmas, including antimatter plasmas, the standard diagnostic techniques used to measure the density and temperature are not appropriate. We present a new method for determining the size, shape, average density, and temperature of a single-component plasma confined in a Penning trap from measurements of the plasma mode frequencies.

PACS numbers: 52.25.Wz, 52.35.Fp, 52.65.+z, 52.70.–m

Many experiments requiring the confinement of charged particles have been performed in Penning traps. High-precision measurements of magnetic moments of fundamental particles [1] have been made, and atomic spectroscopy in an isolated trap environment is of potential use for the next generation of atomic clocks [2]. Similar traps are employed in ion cyclotron mass spectrometry [3], and for experiments on pure electron plasmas [4].

Recently, Penning traps have been used to accumulate antiparticles. Large numbers of positrons have been confined [5], with the goal of studying positron-electron plasmas. These cool positrons have proven useful in the study of positron-molecule interactions [6]. Trapped antiprotons have enabled the precise measurement of the antiproton mass and are required for the formation of antihydrogen [7].

In many of these experiments, the trapped particles form single-component plasmas. Although such work [4,8] has concentrated on cylindrical plasmas, many experiments require a harmonic confining potential, in which the low-temperature equilibria are uniform-density spheroids [9]. A recent cold fluid theory [10] predicts the frequencies of plasma modes in laser-cooled ion plasmas [9,11] and has been used to deduce the aspect ratios of cold, spheroidal electron plasmas [12], but no detailed work on these plasmas at finite temperatures has been carried out.

In this Letter, we present experimental results on the dependence on aspect ratio and temperature of the quadrupole mode frequency in spheroidal electron plasmas. The experiment exploits our new capability of controlling the plasma temperature by rf heating. We compare our results with an analytical model [13] and with numerical simulations. This is the first comprehensive experimental and numerical study to elucidate the shape-dependent effects of plasma temperature on these modes. When extrapolated to $T = 0$, the data agree well with the cold fluid theory. At the experimental temperatures of 300 K and above, the frequencies are found to depend on the plasma temperature, length, and aspect ratio. These results provide a remote, real-time measurement of these

parameters, a capability previously unavailable for electron plasmas and requiring laser systems for ion plasmas. The technique is expected to be particularly useful in the long-term confinement of antiparticles, where dumping the plasma is not desirable, and where the atomic structure required for the laser techniques is absent.

The Penning trap used for these experiments (see Fig. 1) has electrodes that approximate the hyperboloidal surfaces required for a purely quadratic potential. The radial distance from the trap center to the ring electrode is $\rho_0 = \sqrt{2}z_0$, where $z_0 = 6.3$ cm is the distance to each end cap. If the potential on both end caps is U and the ring potential is $-U$, then the potential inside the trap is $\Phi(\rho, z) = U(z^2 - \frac{1}{2}\rho^2)/z_0^2$, where $\rho = (x^2 + y^2)^{1/2}$ is the cylindrical radius. These electrodes are the final stage of a trap for accumulating positrons from a radioactive source [6]. The electron plasmas described here are very similar to the positron plasmas whose study is our main goal, so that the techniques developed for electrons apply to both.

The magnetic field, B, used for these experiments was typically 1 kG, resulting in an electron cyclotron frequency $\Omega_c = eB/mc$ of 1.8×10^{10} rad/s. Here e and m are the charge and mass of the electron, respectively, and c is the speed of light. A trapping potential of $U = -5$ V resulted in a harmonic oscillation frequency $\omega_z = (2eU/mz_0^2)^{1/2}$ of 2.1×10^7 rad/s. Typical plasmas had a length $L \simeq 7$ cm and a radius $\rho_p \simeq 1$ cm,
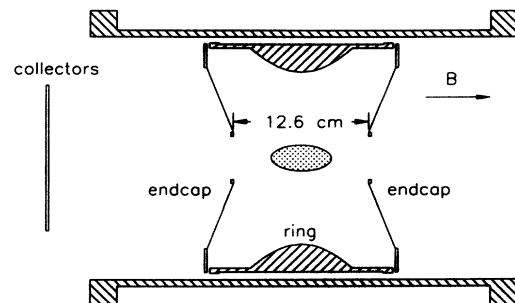

FIG. 1. The Penning trap used for these experiments, with a typical plasma shown to scale.

where we define L and ρ_p as the points at which the particle density $n(\rho, z)$ fell to half its central value n_0. Total particle numbers of $N \simeq 3 \times 10^7$ electrons yielded densities of $n_0 \simeq 2 \times 10^6$ cm^{-3} and plasma frequencies of $\omega_p = (4\pi n_0 e^2/m)^{1/2} \simeq 8 \times 10^7$ rad/s, giving the ordering $\omega_z < \omega_p \ll \Omega_c$. The Debye length was typically $\lambda_D \simeq 1$ mm, so that $\lambda_D \ll \rho_p \ll \rho_0$. The time scale on which the plasma evolves, given by the 1-h radial confinement time for electrons and by the 100 s annihilation time for positrons, is much longer than the other time scales of the experiment, including the 1 s plasma cooling time.

Trapped plasmas cool toward a temperature of $T = 0.025$ eV by collisions with molecules of the N_2 buffer gas (pressure $\simeq 10^{-6}$ torr). To measure the temperature, the plasma is "dumped" through one of the end caps onto a set of concentric rings, where the charge detected gives the number and radial distribution of particles stored. A magnetic field coil to the left of the collectors in Fig. 1 generates the mirror field for a "magnetic beach" temperature analyzer [14]. Plasmas may be heated by applying a short burst ($\Delta t \leq 0.1$ s) of broadband noise ($f < 10$ MHz) to one of the end caps. Figure 2(a) shows the plasma temperature measured during a cycle of rf heating and buffer gas cooling.

Oscillations of the plasma were measured by applying a signal to one of the end caps and detecting the plasma response on the other. A typical spectrum is shown in the inset to Fig. 2(b). The mode labeled f_z was identified as the axial, center-of-mass oscillation because the mea-

sured frequency is very close to the calculated value. The amplitude of the center-of-mass response may be used to determine the total number of particles. An accurate calibration of the response may be obtained by dumping the plasma.

In either trap, when the charge cloud dimensions exceed λ_D, resonances are visible at frequencies both higher and lower than ω_z. In contrast to the center-of-mass mode, the frequencies of these plasma modes are not determined only by the trapping potential, U. In Fig. 2(b), the frequency of the mode designated f_2 in the inset is measured during a heating pulse, showing its clear dependence on temperature. After the plasma cools, the mode frequency returns to its original value, indicating that the plasma shape has not changed significantly. Over longer times, the mode frequency is observed to drift slowly as the plasma expands, providing an example of the use of the mode for real-time monitoring of the plasma. This mode, identified below as the quadrupole mode, was chosen for careful study because it is the most prominent plasma mode and is detectable under a wide variety of plasma conditions, so that parametric dependencies could be studied.

The cold fluid theory of Dubin [10] of modes of a spheroidal single-component plasma is the first analytical theory to treat the boundary conditions of a finite plasma exactly. For strongly magnetized plasmas ($\Omega_c \gg \omega_p$), the cold fluid dispersion relation for low-frequency eigenmodes with azimuthal symmetry reduces to

$$1 - \frac{\omega_p^2}{\omega^2} = \frac{k_2}{k_1} \frac{P_l(k_1)Q_l'(k_2)}{P_l'(k_1)Q_l(k_2)}, \qquad (1)$$

where $k_1 = \alpha(\alpha^2 - 1 + \omega_p^2/\omega^2)^{-1/2}$, $k_2 = \alpha(\alpha^2 - 1)^{-1/2}$, and $\alpha = L/2\rho_p$ is the aspect ratio of the plasma. P_l and Q_l are Legendre functions of the first and second kinds, respectively, and P_l' and Q_l' are their derivatives. Using the cold fluid equilibrium relation [9] for ω_p as a function of ω_z and α, the solutions to Eq. (1) can be expressed as functions of α only, as shown in Fig. 3 for several of the low-order normal modes. For $l > 2$, there are multiple branches of the dispersion relation, corresponding to modes with different numbers of radial nodes. For some plasmas, two low-frequency modes are observed which are candidates for the lower branches of the $l = 3$ and $l = 4$ modes shown in Fig. 3.

The frequency of the mode shown in Fig. 2(b) was studied as a function of the aspect ratio and temperature. The aspect ratio was varied by reducing the magnetic field after loading the electrons, thus expanding the plasma radially. Temperature effects were studied by heating the plasma and measuring the mode frequencies as the plasma cooled, as shown in Fig. 2. Figure 4 shows the second measured mode frequency as a function of temperature for three different plasmas. When the data are extrapolated to $T = 0$, frequencies within about 1% of the cold fluid predictions for the quadrupole ($l = 2$, $m = 0$, in Dubin's notation) mode are obtained,
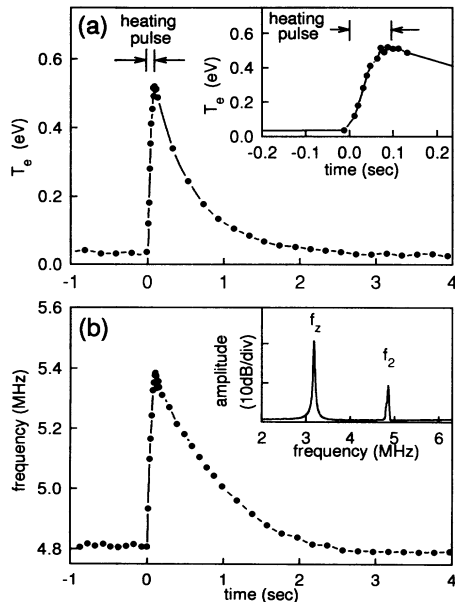

FIG. 2. (a) Temperature measured during a cycle of rf heating and buffer gas cooling. Inset: detail showing temperature rise during the rf pulse. (b) Frequency of the quadrupole mode. Inset: typical spectrum showing center-of-mass mode at $f_z = \omega_z/2\pi$ and quadrupole mode at $f_2 = \omega_2/2\pi$.
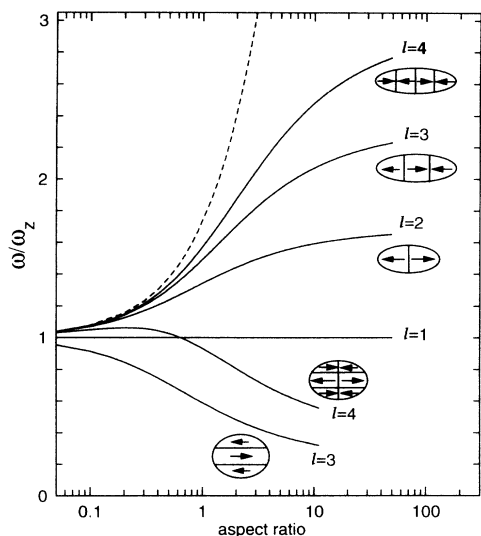
FIG. 3. Dependence of plasma mode frequencies on aspect ratio, according to cold fluid theory. Only the lowest-order azimuthally symmetric modes are shown; for $l = 3$ and $l = 4$, there are two branches. Sketches indicate the fluid motions characteristic of each mode. The dashed line is the plasma frequency.

FIG. 4. Temperature dependence of the quadrupole mode frequency for plasmas with different shapes: (■), $\alpha = 2.24$, $L = 6.20$ cm; (o), $\alpha = 4.38$, $L = 7.52$ cm; and (▲), $\alpha = 7.80$, $L = 8.32$ cm. Solid lines are the results of numerical simulations of the plasmas. Arrows on the vertical axis show the cold fluid theory predictions; dashed lines are from Eq. (2). The inset shows the radial density profiles of these plasmas.

confirming our identification of the mode.

The cold fluid theory assumes a cold plasma of uniform density in an exactly quadratic potential imposed by distant electrodes. To model effects not included in the cold fluid theory, plasmas were simulated numerically. The electrode voltages and z-integrated density profiles of experimentally measured plasmas were used as input to a Poisson-Boltzmann equilibrium code. The resulting equilibria, from which the plasma aspect ratios were obtained, were constrained to match the experimental density profiles and the total particle number. The computations were done assuming axisymmetry and used a 120 by 240 grid for the coordinates ρ and z.

The computed equilibria were then used to create initial distributions for particle-in-cell simulations which used the same spatial grid and electrode representation as the equilibrium computation. The center-of-mass and quadrupole modes were excited by displacing all of the particles by a small amount in the same direction in z and also by stretching the plasma along the z axis. The position of the center of mass, $z_{c.m.}$, and the density-average of the square of the position of the plasma relative to the center of mass, $\langle (z - z_{c.m.})^2 \rangle$, were then tracked in time and Fourier-analyzed to yield the frequencies of the center-of-mass and quadrupole modes, respectively. The plasma was represented by 50 000 particles, which were advanced through 16 384 time steps of 4×10^{-9} s each.

The experimentally measured plasmas shown in Fig. 4 were studied using these simulation techniques. From the Poisson-Boltzmann code, the aspect ratios were found to be 7.80, 4.38, and 2.24. For each aspect ratio, simulations were made for ten temperatures in the range 0.001–0.176 eV. The frequency ratio between the quadrupole and
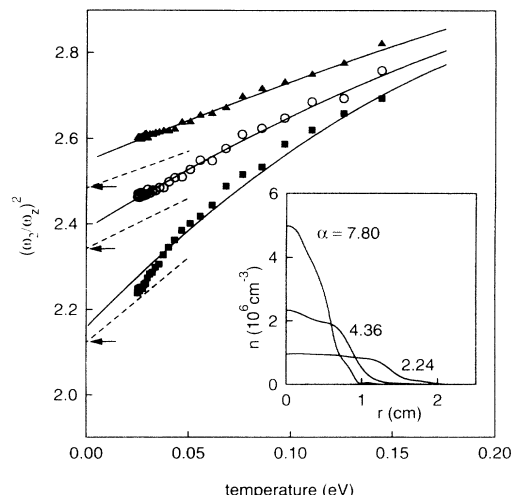
center-of-mass modes shown by the solid lines in Fig. 4 is in excellent agreement with the data. The simulation frequencies at the lowest temperatures agree well with the predictions of Dubin's cold fluid theory, which are marked with arrows on the ordinate of Fig. 4. This is interesting in view of the fact that the density profiles shown in the inset to Fig. 4 differ substantially from the nearly uniform density expected for a plasma in global thermal equilibrium [15] (and assumed by the cold fluid theory). The insensitivity of the mode frequencies to the plasma profile simplifies their use as diagnostics, as discussed below.

An approximate analytical treatment of temperature effects on the quadrupole mode frequency was proposed recently by Dubin [13]. This model leads to a prediction of a shift in the quadrupole mode frequency from the cold fluid result ω_2^c to ω_2 [16]:

$$(\omega_2)^2 = (\omega_2^c)^2 + 20\left[\gamma - g(\alpha)\right] \frac{k_B T}{mL^2}, \qquad (2)$$

with

$$g(\alpha) = \frac{\alpha^2}{2} \frac{\omega_p^2}{(\omega_2^c)^2} \frac{\partial^2 A_3}{\partial \alpha^2}, \qquad (3)$$

where $A_3 = 2Q_1(k_2)/(\alpha^2 - 1)$, k_B is the Boltzmann constant, and $\gamma = 3$ is the ratio of specific heats for one-dimensional expansions. All quantities on the right-hand sides of Eq. (2) and Eq. (3) are evaluated in the cold fluid limit. The function $g(\alpha)$ describes the frequency shift from the temperature dependence of the plasma shape. If this term is neglected, one obtains a result similar to the Bohm-Gross dispersion relation for a warm neutral plasma, $\omega^2 = \omega_p^2 + \gamma k_z^2 k_B T/m$, with $k_z \simeq \pi(l-1)/L$.

The data shown in Fig. 4 indicate that $(\omega_2)^2$ is linear

in T for the longer plasmas studied, but deviates from linearity for the shortest plasma, for which the temperature dependence is strongest. The slopes of the curves at low temperatures agree reasonably well with the predictions of Eq. (2), which are plotted as dashed lines in Fig. 4.

For positron and positron-electron plasmas, nondestructive diagnostics are essential, and the measurement of the frequencies of plasma modes is an attractive way of accomplishing this, because frequencies can be measured with great precision. The modes studied are global, and thus they provide information on global plasma parameters. For the purposes of mode studies, the spatial distribution is adequately parametrized by L and α, since the mode frequencies are relatively insensitive to the radial density profile. Therefore, the cold fluid equilibrium theory for a uniform-density spheroid [9] may be used to relate the parameters N, α, and L:

$$L^3 = \frac{24e^2}{m\omega_z^2}\, k_2^2(\alpha)\, Q_1\left[k_2(\alpha)\right] N. \qquad (4)$$

Thus, a measurement of N fixes a relationship between L and α. Measurement of two plasma modes combined with the results of simulations or warm fluid theory would provide the additional relationships to uniquely determine L, α, and T, and hence also the plasma radius and density. If the temperature is known, as it is in the presence of a buffer gas, then with N determined from the amplitude of the center-of-mass response, Eq. (2) and Eq. (4) may be used to determine L and α from the quadrupole mode frequency. Once the plasma parameters are established, whether by these techniques or by other diagnostics, subsequent changes in either temperature or shape may be deduced from additional shifts in a single mode frequency, as in the data for ω_2 during a heating pulse, shown in Fig. 2(b). Alternatively, if the temperature can be controlled, the plasma length and aspect ratio may be found from the slope and intercept of data for $(\omega_2)^2$ vs T. Applying this technique to the data in Fig. 4, we obtain lengths of 8.5, 7.3, and 5.3 cm for the three plasmas, while the experimental values are 8.3, 7.5, and 6.2 cm, respectively.

The use of data from modes other than the quadrupole mode would benefit greatly from a complete theory of finite-temperature spheroidal plasmas. Modes with azimuthal structure, such as the $l = 2$, $m = 2$ diocotron mode, have frequencies that depend on aspect ratio [10] and could provide the data needed for complete determination of the bulk plasma parameters, if their temperature dependence were understood.

In summary, the data presented here show that the frequency of the quadrupole mode of a spheroidal single-component plasma has well-characterized dependences on the plasma aspect ratio, length, and temperature. These relationships provide a nonperturbative plasma diagnostic that should be useful in a variety of experiments. The excellent agreement between the simulations and the experiment demonstrates that such simulations are a valuable tool for the detailed study of these modes. They could, for example, be used to study the effects of trap anharmonicity, nonuniform plasma density, and nonlinear mode coupling. Based on the results presented here, further work on the theory of plasma modes in finite-temperature spheroidal plasmas is warranted.

[1] H. Dehmelt, Rev. Mod. Phys. **62**, 525 (1990); L. S. Brown and G. Gabrielse, Rev. Mod. Phys. **58**, 233 (1986); D. J. Wineland, W. M. Itano, and R. S. Van Dyck, Jr., Adv. At. Mol. Phys. **19**, 135 (1983).

[2] J. J. Bollinger et al., Phys. Rev. Lett. **54**, 1000 (1985).

[3] C. L. Wilkins et al., Mass Spectrom. Rev. **8**, 67 (1989).

[4] C. F. Driscoll, J. H. Malmberg, and K. S. Fine, Phys. Rev. Lett. **60**, 1290 (1988); C. F. Driscoll and K. S. Fine, Phys. Fluids B **2**, 1359 (1990).

[5] C. M. Surko, M. Leventhal, and A. Passner, Phys. Rev. Lett. **62**, 901 (1989); T. J. Murphy and C. M. Surko, Phys. Rev. A **46**, 5696 (1992).

[6] T. J. Murphy and C. M. Surko, Phys. Rev. Lett. **67**, 2954 (1991); S. Tang et al., Phys. Rev. Lett. **68**, 3793 (1992).

[7] G. Gabrielse et al., Phys. Rev. Lett. **65**, 1317 (1990); G. Gabrielse et al., Phys. Lett. A **129**, 38 (1988).

[8] T. M. O'Neil, Phys. Rev. Lett. **55**, 943 (1985); D. H. E. Dubin and T. M. O'Neil, Phys. Rev. Lett. **60**, 1286 (1988).

[9] J. J. Bollinger et al., Phys. Rev. A **48**, 525 (1993).

[10] D. H. E. Dubin, Phys. Rev. Lett. **66**, 2076 (1991).

[11] D. J. Heinzen et al., Phys. Rev. Lett. **66**, 2080 (1991).

[12] C. S. Weimer et al., "Electrostatic Modes as a Diagnostic in Penning Trap Experiments" (to be published).

[13] D. H. E. Dubin, Phys. Fluids B **5**, 295 (1993).

[14] D. Boyd et al., Phys. Lett. **45A**, 421 (1973).

[15] Local thermal equilibrium along each magnetic field line will be established on a time scale $\tau \simeq 1/\nu_{ee} \simeq 0.1$ ms, where ν_{ee} is the electron-electron collision frequency. This equilibration time is much shorter than the time for cooling on the buffer gas.

[16] D. H. E. Dubin (private communication).